Biosensors and Bioelectronics 152 (2020) 112001

Contents lists available at ScienceDirect

Biosensors and Bioelectronics

journal homepage: http://www.elsevier.com/locate/bios

Construction of flexible enzymatic electrode based on gradient hollow fiber membrane and multi-wall carbon tubes meshes

Huating Huang [a], Tong Li [a], Min Jiang [b], Chenjie Wei [a], Shuyan Ma [a], Dajing Chen [b,**], Weijun Tong [a,***], Xiaojun Huang [a,*]

[a] Department of Polymer Science and Engineering, MOE Key Laboratory of Macromolecular Synthesis and Functionalization, Key Laboratory of Adsorption and Separation Materials & Technologies of Zhejiang Province, Zhejiang University, Hangzhou, 310027, China
[b] School of Medicine, Hangzhou Normal University, Hangzhou, 311121, China

ARTICLE INFO

Keywords:
Flexible biosensor
Enzyme micro-particle
Carbon nanotube
Hollow fiber

ABSTRACT

In this study, we developed a convenient way to construct a flexible enzymatic electrode with excellent stability and electrochemical performance for implanted glucose monitoring. The electrode was constructed through the co-immobilization of the glucose oxidase micro-particles (GOD MPs) and multi-wall carbon nanotubes (CNT) on the inner surface of a gradient-structured hollow fiber membrane (GHM), where CNT improved the electron transport efficiency and GHM controlled the transfer of substances and interferences. GOD MPs showed higher stability under various operation conditions than the free enzymes due to the $MnCO_3$ template method, which enabled the biosensor to remain relative sensitivity at >86% over 9 days. The GOD MPs biosensor also showed high selectivity, reproducibility, and linear sensing range from 0 mM to 24 mM ($R^2 = 0.9993$) with a current sensitivity of 25 nA/mM. The combination of porous-structured membrane and the flexible CNT meshes ensures the electrical connections and sensing accuracy of the biosensor under the deformation status. In-vivo experiments showed reliable current responses to variations in blood glucose concentrations that were consistent with tail blood test results. This co-immobilization of enzyme micro-particles in the 3D porous structure method developed a bio-composite platform technology towards the applications in flexible sensing and implantable medical devices.

1. Introduction

Diabetes mellitus is one of the most serious chronic diseases and causes severe complications with negative impacts on the patient's health (Elsherif et al., 2019; Rogers, 1994). A reliable continuous glucose monitor (CGM) can help patients monitor fluctuations in their blood glucose levels through a timely alert for hypoglycemia (<3.0 mM) or hyperglycemia (>7.2 mM) (Bolinder et al., 1997; Chen et al., 2017). Non-invasive CGM sensors are easy to operate with a low risk of infection (Lee et al., 2018) by analyzing biological fluids such as tears, saliva, and sweat (Vashist, 2012). However, they still face the obstacles of low accuracy and insufficient reliability because the concentration of glucose in these biological fluids is only 1–10% of that in the blood (Kiang et al., 2017; Vashist and Luong, 2017.). Therefore, an implantable CGM device that can directly monitor a patient's blood or interstitial fluid glucose level is a more practical option than the non-invasive CGM (Heller and Feldman, 2008; Vashist, 2013).

Studies on enzyme-amperometric electrochemical CGM biosensors based on the glucose oxidase (GOD) have revealed its high selectivity and sensitivity (Orleans, 1973; Sabu et al., 2019). However, deactivation and leakage of GOD often led to the low stability and limited longevity of the sensors (Bankar et al., 2009; Tse and Gough, 1987; Zhang et al., 1994). Theoretically, improving the immobilization method (Salek-Maghsoudi et al., 2018) is an effective solution. In general, physical immobilization methods like physical entrapment can preserve massive amounts of enzymes and maximize enzyme activity but suffers from drawbacks such as enzyme leakage (Sternberg et al., 1988; Sakai et al., 2010). Chemical methods like covalent binding can help enzymes gain high stability by minimizing enzyme folding at the expense of partial activity loss (Cosnier, 2014). Therefore, combining the advantages of

* Corresponding author., Lab 249 of No.7 teaching building, Xixi campus of Zhejiang University, Hangzhou, 310028, China
** Corresponding author.
*** Corresponding author.
E-mail addresses: djchen@hznu.edu.cn (D. Chen), tongwj@zju.edu.cn (W. Tong), hxjzxh@zju.edu.cn (X. Huang).

https://doi.org/10.1016/j.bios.2019.112001
Received 18 October 2019; Received in revised form 21 December 2019; Accepted 27 December 2019
Available online 28 December 2019
0956-5663/

physical and chemical methods would be desirable for simultaneous desorption and deactivation of enzymes.

Other challenges associated with the implanted enzymatic CGM are poor linearity and narrow sensing range caused by oxygen deficiency in interstitial environment (Chen et al., 2015; Sabu et al., 2019). In this case, permselective coatings were introduced to limit the diffusion of substrates (Chen et al., 2015; Lin et al., 2004). Researchers have also found that polymer coatings can eliminate biomolecular interferences by changing interference transport properties based on polarity, size, or charge (Kotanen et al., 2012), and the use of porous films (porosity diameter < 6 μm) can minimize the foreign body response by blocking the infiltration of inflammatory cells which ultimately improves sensor's biocompatibility (Nichols et al., 2013; Soto et al., 2017). In our previous research on implanted enzymatic electrodes, we employed a hollow fiber membrane as the permselective membrane and proved its feasibility of in-vivo experiments (Zhou et al., 2019). However, the electrode was based on a rigid stainless needle, which resulted in uncomfortable to wear and increases the possibility of infection.

In this work, we report a new strategy for constructing a flexible enzymatic electrode based on GHM with high stability and electrochemical performance that involves co-immobilizing glucose oxidase micro-particles (GOD MPs) made by the $MnCO_3$ template with multi-wall carbon tubes (CNT). The template method allows massive enzymes to be crosslinked in a restricted space and provides efficient protection for the active sites of enzymes during the fabrication, resulting excellent enzyme stability of GOD MPs under different temperature, pH, operation cycle, and storage conditions. Next, due to the CNT's unique superiorities including high electrical conductivity, rapid electrode kinetics, excellent electrocatalysis activity, chemical stability, and mechanical strength (Ajayan, 1999; Luong et al., 2017; Vashist et al., 2011a; Xu et al., 2019), we constructed porous conductive CNT 3D-meshes between GOD MPs and the electrodes to entrap GOD MPs and realize electrocatalysis. We further investigated the in-vitro electrochemical performance of the prepared electrode concerning sensitivity, storage time, selectivity, and deformation performance. There was an excellent linearity ($R^2 \geq 0.999$) fitting to stable output current in response to the addition of glucose (0 mM–24 mM), both in normal and deformed states of the biosensor. Finally, by mounting the biosensor on rat's back, the in-vivo experiments proved the ability of monitoring glucose level changes in interstitial fluid.

2. Experiment

2.1. Materials

Glucose Oxidase from *Aspergillus niger* (GOD, 360 U/mg) was purchased from BBI Solutions (Gwent, NP4 9RL, UK). Horseradish peroxidase (HRP) was purchased from Yuanye Biotechnology Co. Ltd. Lactate (LAC), uric acid (UA), ascorbic acid (AA), acetaminophen (AP) and 2,2′-Azinobis (3-ethylbenzthiazoline-6-sulphonate) (ABTS) were purchased from Aladdin Biochemical Technology Co., Ltd. Glycine, polyallylamine hydrochloride (PAH) (Mw 17,500), poly sodium 4-styrenesulfonate (PSS) (Mw 70,000), glutaraldehyde (GA), fluorescein isothiocyanate (FITC), and multi-walled carbon tubes (CNT, 50 nm in diameter and 10 μm in length, 10 wt%) were purchased from Sigma-Aldrich Technology Co., Ltd. Glucose monohydrate, and paraffin wax were purchased from Macklin Biochemical Co., Ltd. Coomassie Brilliant Blue-G250, ethylene diamine tetraacetic acid (EDTA), $MnCl_2$, $NaCO_3$, Na_2HPO_4, $KH_2PO_4{\cdot}H_2O$, Pt wire (0.2 mm diameter), and ethanol were purchased from Sinopharm Chemical Reagent Co., Ltd. Polysulfone hollow fibrous membranes (GHM) were afforded by O'happure Membrane Technology Co., Ltd. (Nanjing, China).

2.2. Fabrication of GOD MPs and biosensor working electrodes

2.2.1. Fabrication of GOD MPs

An equal volume of 0.2 M Na_2CO_3 and 0.2 M $MnCl_2$ containing 2.5 mg/ml of GOD and 5 mg/ml of BSA were mixed in a beaker and stirred at 1000 rpm for 1 min at 25 °C until the GOD & BSA-doped $MnCO_3$ submicrometer templates were ultimately formed. Next, the templates were incubated in 2 mg/ml PSS, 2 mg/ml PAH, and 2 mg/ml PSS solutions tandemly for 15 min to form a PSS-PAH-PSS multilayer film outside the template through the layer-by-layer assembly method (Li et al., 2019). Next, the templates were incubated in GA solution for 1 h to cross-link GOD with BSA and then treated with 2 mg/ml of glycine solution for 1 h to eliminate any excess aldehyde. Subsequently, the templates were incubated in 0.1 M of EDTA for 15 min to corrode the $MnCO_3$ (Li et al., 2017). Finally, the obtained GOD MPs were further washed until neutral and finally dispersed in water at 4 °C. All the incubations were performed under gentle shaking conditions, followed by a thorough wash before the next step.

2.2.2. Fabrication of biosensor working electrodes

A 6 cm long GHM was sheathed on a dispensing needle (#28) and fixed with glue. The end of the GHM was sealed with paraffin wax to retain a sufficient length of 5 cm. Subsequently, a 50 μl mixture of 1% ultrasonic dispersive CNT and 2 mg/ml of GOD MPs or free GOD at a ratio of 2:1 by volume was driven into the GHM using a propelling pump. The GHM was removed from the dispensing needle after immobilization, and a Pt wire was inserted into the hollow structure of the enzyme-deposited GHM as an electrical connection between the CNT meshes and the electrochemical working station. Enzymatic electrodes made by GOD MPs and free GOD were called GOD MPs/CNT@GHM and free GOD/CNT@GHM, respectively.

2.3. GOD MPs performance test

The performance of GOD MPs was first evaluated after they were immobilized in GHM (GOD MPs@GHM). Free GOD immobilized by GA on GHM (free GOD@GHM) was used as the control group in this experiment. Enzyme loading stability was investigated by studying the dependence of enzyme leakage on wash time for 140 min under 0.06 MPa. PH stability was evaluated after incubating samples in buffers from pH 3 to pH 9 for 2 h. Thermal stability was investigated by studying the heating time dependent enzyme activity at 60 °C for 12 h. Operation stability and storage stability of GOD MPs were investigated by studying operation time dependent enzyme activity every 11 h for a total of seven times at 37 °C and the storage time dependent enzyme activity for 30 days at 4 °C, respectively. The stability was evaluated on the basis of the relative activity (the ratio of residual activity to initial activity) based on a previously-reported method using ABTS as a reagent (Re et al., 1999). Experimental details about the stability test method are provided in Table S1.

2.4. Glucose biosensor test

2.4.1. In-vitro biosensor test

All in-vitro measurements were carried out under ambient temperature using a CHI660 electrochemical workstation with a two-electrode system at a potential of 0.33 V. Enzyme immobilized GHM was used as a working electrode, and Pt wire was used as the reference and counter electrode. To obtain the corresponding current curves for different concentrations of glucose, 2 mM of glucose solution was added every 300 s. To evaluate the storage stability of the biosensor, the current signal for 2 mM glucose was collected every two days. The electrode was stored at 4 °C after being thoroughly washed and naturally dried after each test. For the interference test, the current signal was collected when interfering substrates, including LAC (1 mM), UA (1 mM), AA (0.1 mM), AP (0.1 mM), and glucose (1 mM), were added for contrast. More

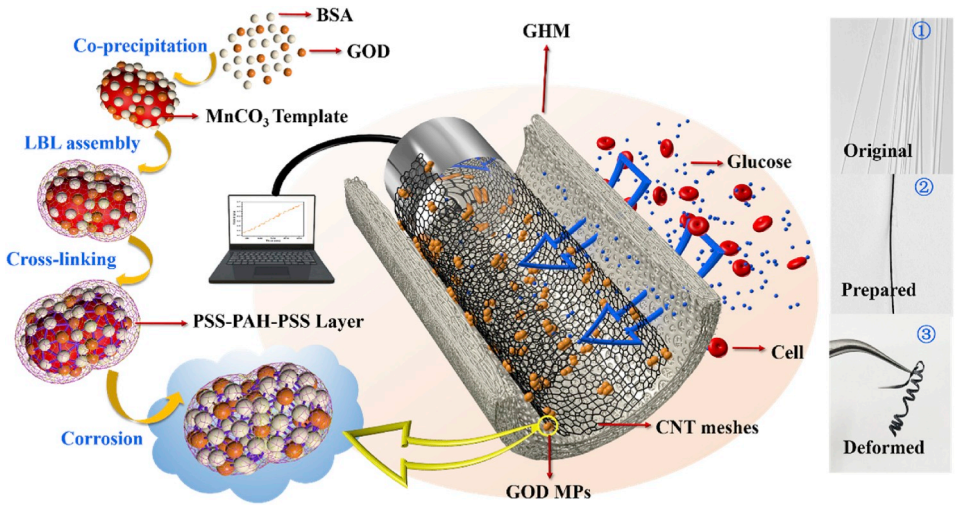

Scheme 1. Diagrammatic sketch of the preparation of GOD MPs (left) and the working electrode of the biosensor (middle); pictures of the original GHM, prepared enzymatic electrode and the deformed electrode (right).

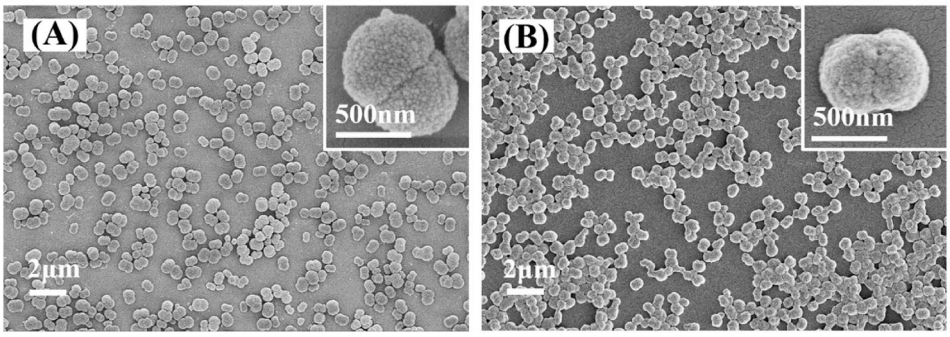

Fig. 1. Scanning electron microscopy (SEM) (S4800, HITACHI) images of GOD MPs with (A) and without (B) $MnCO_3$ template.

interferences were investigated in Table S8 (Zheng et al., 2012). For the deformation test, the current signal was collected before and after deformation using the same electrode. For the reproducibility test, eight biosensors made in the same way were used to measure 1 mM glucose and the currents were collected to assess the relative standard deviation (RSD).

2.4.2. *In-vivo biosensor test*

Male Sprague-Dawley rats (170 g) were anesthetized via intraperitoneal injection of 1% Pentobarbital (10 μl/g). The GOD MPs/CNT@GHM biosensor electrode and Pt wire were carefully implanted into the backs of rats, as shown in Fig. 5A. A lab-made data acquisition system was connected to the two electrodes and mounted on the rat's back. After the current stabilization period (1 h), glucose solution (300 mg/kg) and insulin (0.5 unit/kg) were respectively injected to cause a rapid change of the rat's blood glucose concentration. A glucose test strip (Onetouch Ultra) was used to measure the glucose concentration in the tail vein blood of the rat. The first strip reading was used to calibrate the sensor current with the actual blood glucose levels. The test strip measurements were used to compare sensor current changes to verify the effectiveness of the system. All in-vivo experiments were approved by the human and animal ethics committee of Hangzhou Normal University.

3. Result and discussion

3.1. *Characterization*

3.1.1. *Characterization of GOD MPs*

As illustrated in Scheme 1, GOD MPs were fabricated using a co-precipitation method in which $MnCO_3$ was used as the template and GA was used as the cross-linker. The influence of the mass ratio of GOD to BSA and the concentration of GA were investigated. According to Fig. S2, when treated with 0.5% GA, GOD MPs exhibited increased activity and a stable structure at a mass ratio of 1:2 (GOD: BSA). Such mass ratio and GA concentration were employed throughout the research.

As shown in Fig. 1A, the size of the $MnCO_3$ template containing GOD and BSA was 859 ± 62 nm. The surface of the peanut-like template was rough and contained nanoparticles, as shown in Fig. 1A (inset). The PAH-PSS-PAH self-assembled layer vested the micro-particles with a negative electron layer around 5 nm in thickness, which resulted in excellent capsulation for enzymes and superior dispersion in water (Tong et al., 2012). After the removal of $MnCO_3$ via EDTA treatment, the obtained GOD MPs had a dimension of 721 ± 54 nm (Fig. 1B) and a smooth surface with a similar shape to the templates (Fig. 1B (inset)). The Energy-dispersive X-ray spectroscopy results showed that the manganese in final GOD MPs could be barely detected, confirming the complete removal of $MnCO_3$ (Fig. S3).

3.1.2. *Characterization of co-immobilization of GOD MPs and CNT on GHM*

The porosity of GHM decreased slightly (about 3.6%) after GOD MPs

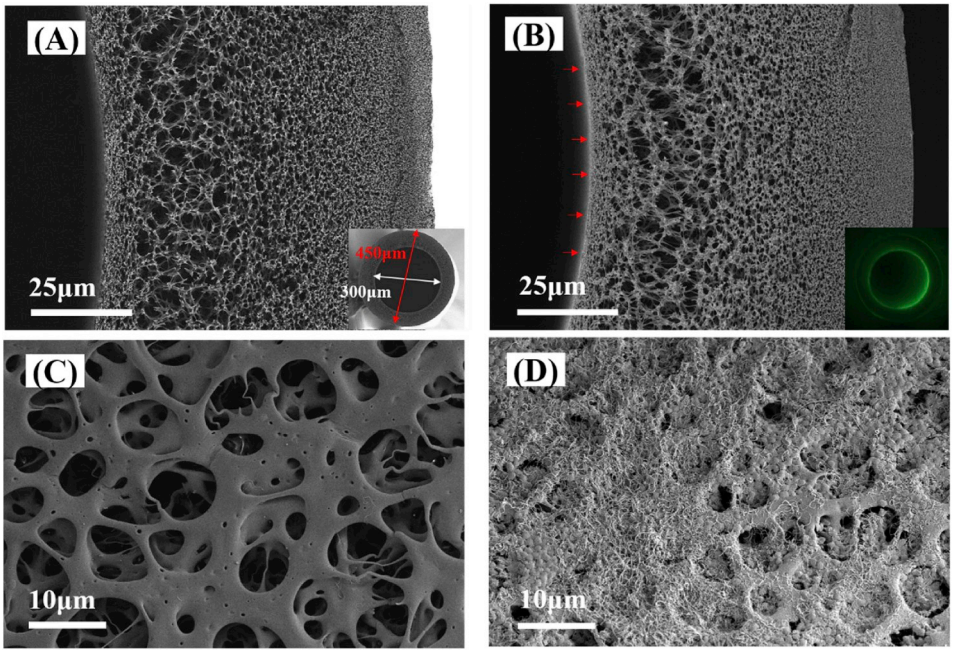

Fig. 2. Cross-section SEM images of GHM before (A) and after (B) GOD MPs & CNT were immobilized; SEM images of the inner surface of GHM before (C) and after (D) GOD MPs and CNT were immobilized.

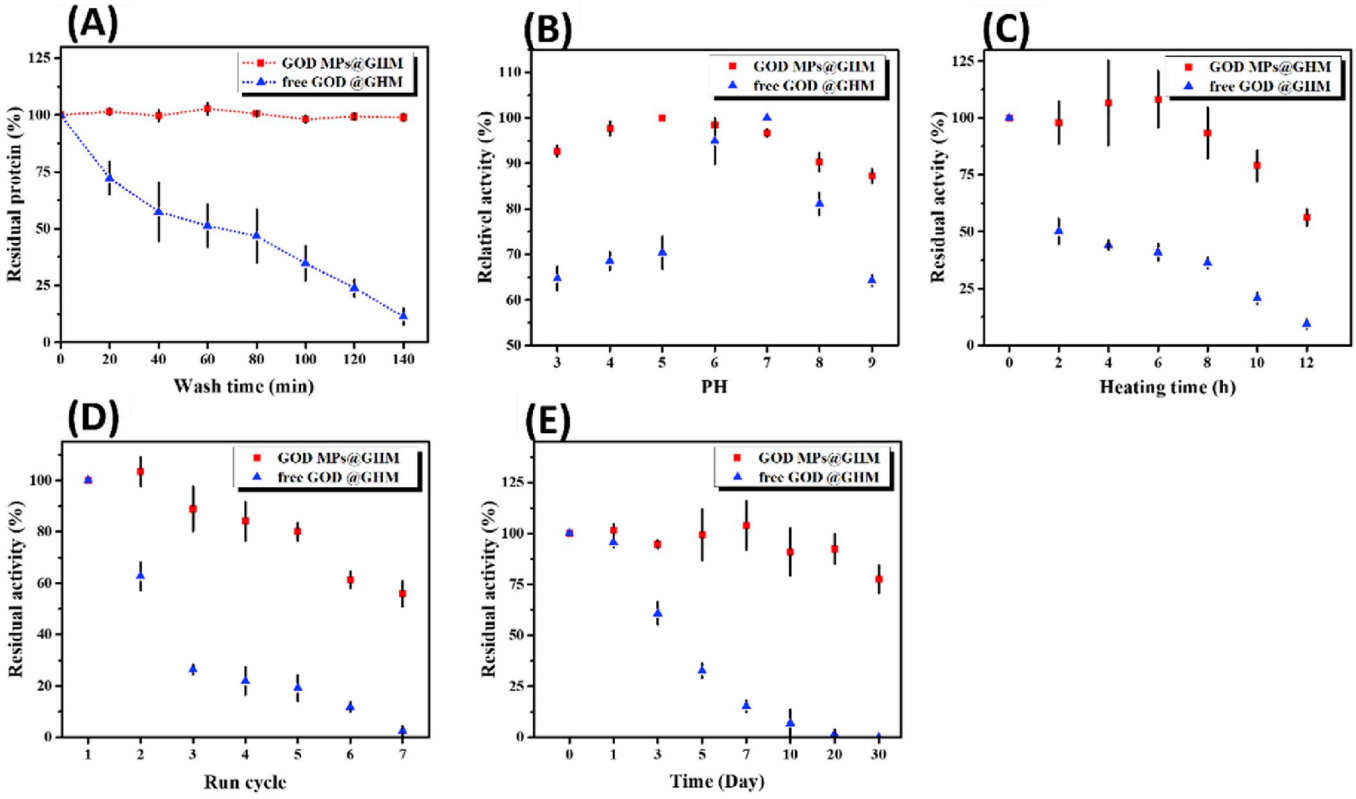

Fig. 3. Loading stability (A), pH stability (B), thermal stability (C), operational stability (D), and storage stability (E) of GOD MPs@GHM and free GOD@GHM.

and CNT immobilized, and its pore size distribution hardly fluctuates within the error range (Fig. S4) when compared with blank GHM measured by mercury intrusion porosimetry (AutoPore IV 9500). As shown in Fig. 2A (inset), GHM had an average inner diameter of about 300 μm and an average outer diameter of about 450 μm. It was covered with large-sized holes of 7.76 ± 0.80 μm on the inner surface (Fig. 2C), and smaller holes on the outside surface of 0.64 ± 0.11 μm in diameter (Fig. S5). Such a hollow gradient structure (Fig. 2A) can efficiently resist the leakage of enzyme and the invasion of macrophages that polluted the sensing area (Heller, 1999). Fig. 2B shows the mixture of GOD MPs and CNT formed a thin layer (about 1 μm thick) on the inner surface of GHM (Fig. S6), which was also confirmed by using fluorescence microscopy

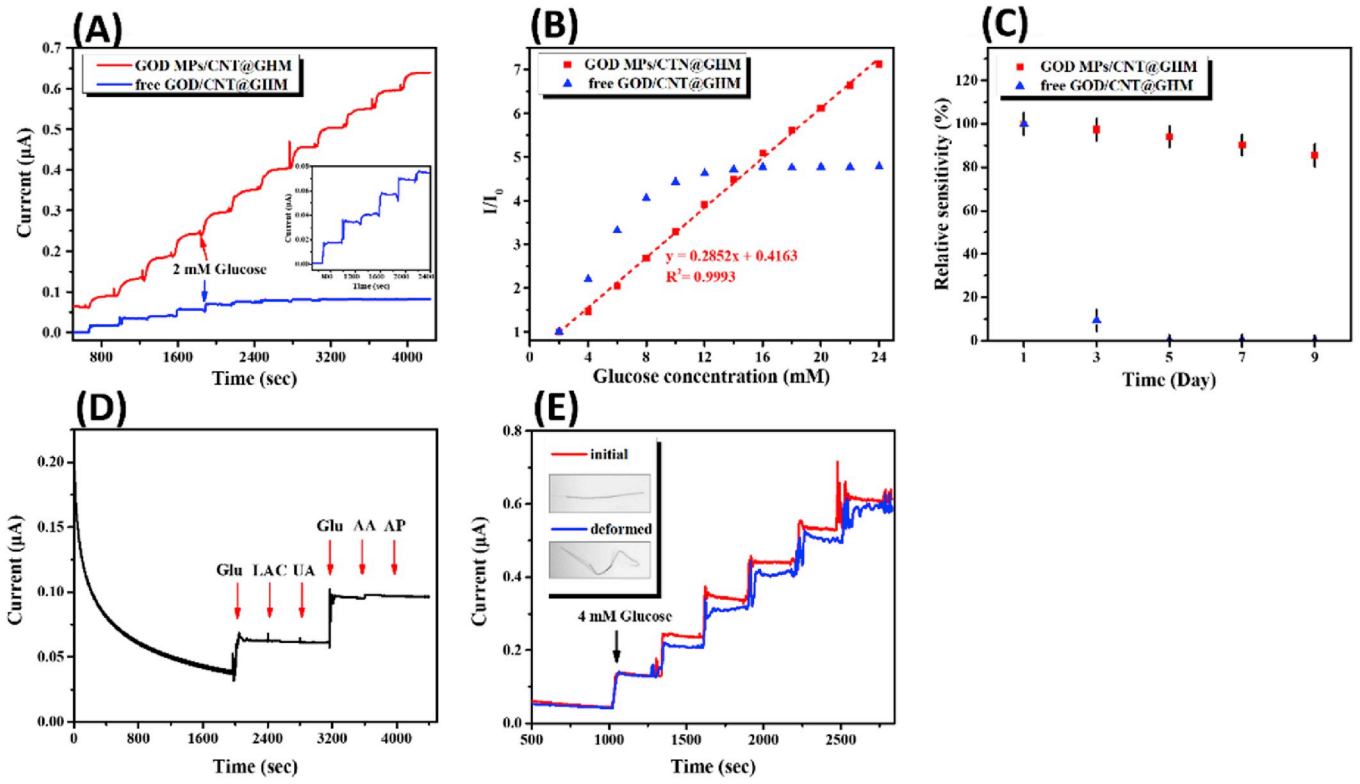

Fig. 4. In-vitro tests. Amperometric responses to various concentrations of glucose (A) and its fitting curve (B); the storage stability of electrodes (C); interference test of prepared GOD MPs/CNT@GHM electrode with 1 mM glucose (twice) and other interfering substances (1 mM LAC, 1 mM UA, 0.1 mM AA and 0.1 mM AP) (D); amperometric responses to various concentrations of glucose of the flexible GOD MPs/CNT@GHM electrode in the deformation test (E).

(Nikon Eclipse Ti–S) observing FITC labeled GOD MPs (Fig. 2B (inset)). Fig. 2D shows that this mixture layer was a porous network instead of a dense cake layer. CNT was intertwined to create 3D-meshes among the dispersed GOD MPs (Fig. S7), which could effectively promot the circulation of the liquids, constraint GOD MPs and establish conductive channels for electrical transports between GOD MPs and the electrode.

3.2. Activity and stability of immobilized GOD MPs

The leakage, unfolding, and inactivation of the enzymes are responsible for the short lifespan of sensors and the irreproducibility of results (Vashist et al., 2011b). The delamination and time-temperature dependent changes of the membrane also present challenges in the implementation of biosensors. In this case, we investigated the stability of GOD MPs that were immobilized on the GHM (GOD MPs@GHM) comparing with free GOD that was immobilized on the GHM (free GOD@GHM).

In contrast to the 11% residual amount of free GOD as shown in Fig. 3A, GOD MPs remained at 99% under the same conditions which supported the fact that GOD MPs would hardly leach under prolonged high-pressure scouring. This is because the size of the GOD MPs enabled them to fit into the intricate meshes of CNT. Furthermore, even if GOD MPs leached into GHM, the gradient structure would trap the leaked particles inside the hollow chamber. Fig. 3B shows that both samples can remain >95% of the highest activity at pH 6 and 7. However, in other pH ranges, the activity of the free enzyme rapidly dropped below 70% of the highest activity while GOD MPs@GHM could remain above 92.7% of the highest activity under acidic conditions and above 87.2% under alkaline conditions. Fig. 3C illustrates that GOD MPs@GHM minimally decreased to 97.9% of initial activity after 2h of heating and 56.2% after 12h whereas free GOD@GHM dove to 50.2% and 9.4%, respectively. The increase in enzyme tolerance to a wide pH range and high temperature can be attributed to the decrease in buffer penetration and the minimized enzyme unfolding imposed by the immobilization method in the confined $MnCO_3$ template. Compared to free GOD@GHM, which was hardly surviving at the end of both experiments shown in Fig. 5D and E, GOD MPs@GHM was found to maintain 55.8% of its initial activity after seven cycles of reuse and 77.6% activity after 30 days of storage. The high level of operational reusability and excellent storage stability of GOD MPs is an essential feature for its potential application in the biosensor industry. This is mainly because the entrapment of enzymes in the $MnCO_3$ template prevents its aggregation and provides a protective environment that limits the denaturation factors. Moreover, the macroscopic morphology of the GHM did not significantly change in the above extreme condition tests, which supported its favorable implementation under different operation conditions.

3.3. Electrochemical test on GOD MPs/CNT@GHM

3.3.1. In-vitro experiment

Glucose oxidase enzyme, in the presence of dissolved molecular oxygen, produces hydrogen peroxide that may be oxidized anodically at CNT surfaces with positive potential. As shown in Fig. 4A, the current response of both electrodes steeply increased with the addition of glucose solution. However, the current signal of GOD MPs (0.025 μA/mM) was an order of magnitude larger than that of free GOD (0.009 μA/mM) due to the high loading capacity of GOD MPs on the unit length of GHM. For GOD MPs electrodes, the current of each glucose concentration increase was regular and stable while the current of the free GOD electrode was irregular and unstable (Fig. 4A (inset)). The current of GOD MPs/CNT@GHM showed an excellent linear relationship with the concentration of added glucose (from 0 to 24 mM), and the fitting curve of the linear correlation coefficient was 0.9993 (Fig. 4B). The possible reasons for the extended sensing linear range of glucose were, first, the fact that enzyme activity and stability were maintained at the highest levels and, second, the fact that GOD MPs were heavily loaded in the

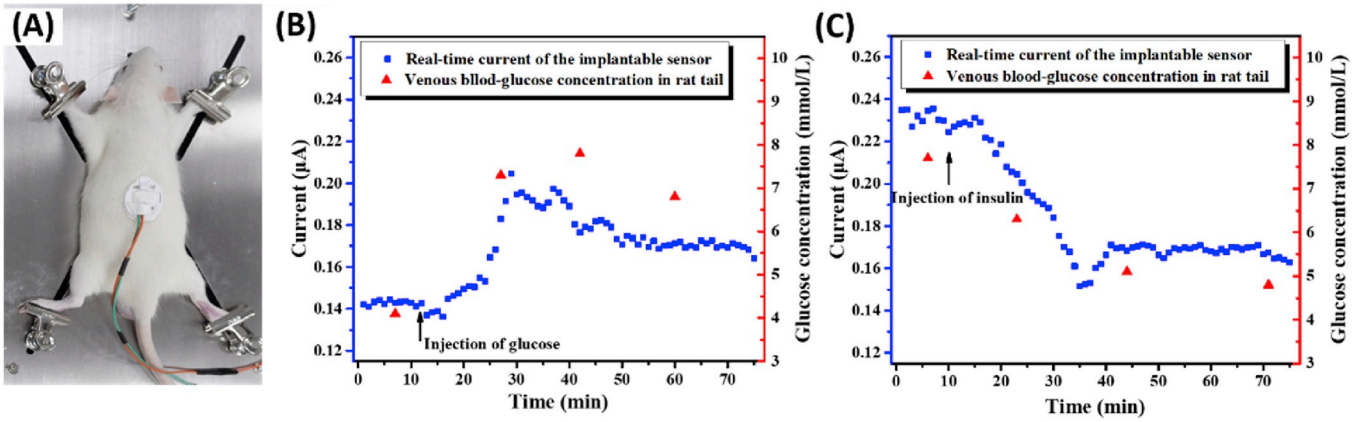

Fig. 5. In-vivo test in rats. Image of transcutaneous glucose biosensor attachment to the rat's back (A); implanted sensor current response to glucose injection (B) and insulin injection (C) and tail vein blood test.

confined space inside the membrane while on the outside, the diffusion of the glucose was limited by GHM, allowing the redox reaction to proceed sufficiently. Third, the CNT meshes catalyzed the formation of electrons and accelerated the transmission of electrons from enzymes to the working electrode.

Biosensors inevitably have the problem of enzyme inactivation, the sensitivity of the free GOD electrode declined sharply to 9.4% on the third day and the electrode was completely unresponsive after 9 day as shown in Fig. 4C. Meanwhile, the sensitivity of GOD MPs/CNT@GHM electrode decreased slowly from the first day to the ninth day and ultimately remained constant at 85.5% of the initial sensitivity. This significant sensitivity advantage of GOD MPs based biosensor could ascribe to the stabilities that the $MnCO_3$ template method brought. Fig. 4D presents the amperometric responses of major potential electroactive species, the prepared GOD MPs based biosensor hardly gives a significant response to LAC, UA, AA, and AP whereas it shows high sensitivity to glucose solution. More interferences including salicylate, creatinine, bilirubin, nitrite, serotonin, paracetamol, dopamine, and peroxynitrite were tested. The sensitivity was expressed as the logarithmic ratio of interference and glucose sensitivity and the sensitivities ranged from −3.2 to −5.1 as shown in Table S8, which verified the selectivity of the biosensor due to the reliable permselectivity of GHM.

The electrochemical performance of the electrode under deformation was investigated to measure its flexibility. As shown in Fig. 4E (inset), the biosensor was squashed and bent in contrast to the initial state, but its electrochemical signal was slightly lower (Fig. 4E) and still maintained an excellent correlation of $R^2 = 0.9986$ compared to $R^2 = 0.9990$ before deformation (Fig. S9). Because the sparse and conductive CNT meshes equivalently extended the tail end of the hard electrode and changed the method of electrons transferring between enzymes and the electrode that allowing GHM to exert its flexible characteristics from the face-to-face connection that used in our previous research (Zhou et al., 2019) into plot-to-plot touch. Moreover, due to the simple one-step immobilization of enzyme particles and CNT meshes, high reproducibility can be achieved and the relative standard deviation (RSD) was 4.7% obtained by measuring currents of eight GOD MPs/CNT@GHM electrodes.

3.3.2. *In-vivo experiment*

The capability to monitor changes in blood glucose in-vivo was evaluated in this experiment through the response current detected in an implanted biosensor made of GOD MPs/CNT@GHM electrode under the subcutaneous tissue of an anesthetized, non-diabetic rat (Fig. 5A). The real-time current of the sensor can be converted into a glucose concentration value by multiplying the currents by a constant, which calibrated based on the first blood sample that withdrawn. After the injection of glucose solution, the biosensor's response current rapidly increased in 20 min and then gradually decreased as Fig. 5B shown. The biosensor's current rapidly reduced after injection of insulin and then maintained at a low level (Fig. 5C). The change of the biosensor's current in both comparisons closely followed the blood glucose trend discretely sampled in the rat tail by a glucose meter. Besides, a response current appeared in less than 50 s after injecting the rat with glucose or insulin, which is a relatively quick response time compared to those of partial biosensors. Concerning the original current signal, the in-vivo experiment demonstrates that the implanted biosensor based on GOD MPs/CNT@GHM can effectively monitor blood glucose changes in real-time.

4. Conclusion

In this study, a novel flexible enzymatic electrode was developed by entrapping template-based GOD MPs in CNT meshes modified GHM. The $MnCO_3$ template method enabled GOD to retain maximal stability while not hindering the interaction between analytes and enzyme active sites. The CNT modified GHM served as a selective diffusion layer that guaranteed the minimal leakage of enzymes, as well as a conductive and catalytic flexible substrate that improved the current transmission efficiency of the biosensor. The in-vitro tests showed that the biosensor has high selectivity, reproducibility, flexibility, and excellent sensing linearity from 0 to 24 mM ($R^2 = 0.9993$). The in-vivo experiment in rats verified the feasibility of the use of flexible sensor monitoring for changes in blood glucose levels. In the long term, we expect this structure to serve as a platform technology for the application of implantable devices for diabetes management as well as other medical diagnoses. So we will continue to improve electron transport efficiency by establishing a cascade system in the enzyme MPs and verify the universality of this platform technology for other enzyme based sensors for flexible electronics applications.

Declaration of competing interest

The authors declare that they have no known competing financial interests or personal relationships that could have appeared to influence the work reported in this paper.

CRediT authorship contribution statement

Huating Huang: Methodology, Investigation, Data curation, Writing - original draft. **Tong Li:** Investigation. **Min Jiang:** Investigation. **Chenjie Wei:** Writing - review & editing. **Shuyan Ma:** Writing - review & editing. **Dajing Chen:** Conceptualization, Project administration, Writing - review & editing, Resources. **Weijun Tong:** Project administration, Resources. **Xiaojun Huang:** Conceptualization, Supervision,

Writing - review & editing, Resources.

Acknowledgment

The work was financially funded by National Natural Science Foundation of China (Grant No. 61801160), Zhejiang Provincial Natural Science Foundation of China (Grant No.LY18H180009) and the Fundamental Research Funds for the Central Universities of China (Grant No.2018QNA4057).

Appendix A. Supplementary data

Supplementary data to this article can be found online at https://doi.org/10.1016/j.bios.2019.112001.

References

Ajayan, P.M., 1999. Chem. Rev. 99, 1787–1799.
Bankar, S.B., Bule, M.V., Singhal, R.S., Ananthanarayan, L., 2009. Biotechnol. Adv. 27, 489–501.
Bolinder, J., Hagström-Toft, E., Ungerstedt, U., Arner, P., 1997. Diabetes Care 20 (1), 64–70.
Chen, C., Zhao, X.L., Li, Z.H., Zhu, Z.G., Qian, S.H., Flewitt, A.J., 2017. Sensors (Switzerland) 17, 1–19.
Chen, D., Wang, C., Chen, W., Chen, Y., Zhang, J.X.J., 2015. Biosens. Bioelectron. 74, 1047–1052.
Cosnier, S., 2014. Electrochem. Biosens. 1–398.
Elsherif, M., Hassan, M.U., Yetisen, A.K., Butt, H., 2019. Biosens. Bioelectron. 137, 25–32.
Heller, A., 1999. Annu. Rev. Biomed. Eng. 1, 153–175.
Heller, A., Feldman, B., 2008. Chem. Rev. 108, 2482–2505.
Kiang, T.K.L., Ranamukhaarachchi, S.A., Ensom, M.H.H., 2017. Pharmaceutics 9 (4), 43.
Kotanen, C.N., Moussy, F.G., Carrara, S., Guiseppi-Elie, A., 2012. Biosens. Bioelectron. 35, 14–26.
Lee, H., Hong, Y.J., Baik, S., Hyeon, T., Kim, D.H., 2018. Adv. Healthc. Mater. 7, 1–14.
Li, H., Xiong, Y., Zhang, Y., Tong, W., Georgieva, R., Bäumler, H., Gao, C., 2017. Macromol. Chem. Phys. 218, 1–6.
Li, T., Li, J., Pang, Q., Ma, L., Tong, W., Gao, C., 2019. ACS Appl. Mater. Interfaces 11, 6789–6795.
Lin, Y., Lu, F., Tu, Y., Ren, Z., 2004. Nano Lett. 4, 191–195.
Luong, J.H.T., Glennon, J.D., Gedanken, A., Vashist, S.K., 2017. Microchim. Acta 184, 369–388.
Nichols, S.P., Koh, A., Storm, W.L., Shin, J.H., Schoenfisch, M.H., 2013. Chem. Rev. 113, 2528–2549.
Orleans, N., 1973. Anal. Chim. Acta 64 (3), 439–455.
Re, R., Pellegrini, N., Proteggente, A., Pannala, A., Yang, M., Rice-Evans, C., 1999. Free Radic. Biol. Med. 9, 1231–1237.
Rogers, D.G., 1994. Clin. Pediatr. (Phila).
Sabu, C., Henna, T.K., Raphey, V.R., Nivitha, K.P., Pramod, K., 2019. Biosens. Bioelectron. 141, 111201.
Sakai, S., Liu, Y., Yamaguchi, T., Watanabe, R., Kawabe, M., Kawakami, K., 2010. Biotechnol. Lett. 32, 1059–1062.
Salek-Maghsoudi, A., Vakhshiteh, F., Torabi, R., Hassani, S., Ganjali, M.R., Norouzi, P., Hosseini, M., Abdollahi, M., 2018. Biosens. Bioelectron. 99, 122–135.
Soto, R.J., Hall, J.R., Brown, M.D., Taylor, J.B., Schoenfisch, M.H., 2017. Anal. Chem. 89 (1), 276–299.
Sternberg, R., Bindra, D.S., Wilson, G.S., Thévenot, D.R., 1988. Anal. Chem. 60, 2781–2786.
Tong, W., Song, X., Gao, C., 2012. Chem. Soc. Rev. 41, 6103–6124.
Tse, P.H.S., Gough, D.A., 1987. Biotechnol. Bioeng. 29, 705–713.
Vashist, S., 2013. Diagnostics 3, 385–412.
Vashist, S.K., 2012. Anal. Chim. Acta 750, 16–27.
Vashist, S.K., Luong, J.H., 2017. Point-of-care Glucose Detection for Diabetic Monitoring and Management. CRC Press.
Vashist, S.K., Zheng, D., Al-Rubeaan, K., Luong, J.H.T., Sheu, F.S., 2011a. Biotechnol. Adv. 29, 169–188.
Vashist, S.K., Zheng, D., Al-Rubeaan, K., Luong, J.H.T., Sheu, F.S., 2011b. Anal. Chim. Acta 703, 124–136.
Xu, S., Zhang, Y., Zhu, Y., Wu, J., Li, K., Lin, G., Li, X., Liu, R., Liu, X., Wong, C.P., 2019. Biosens. Bioelectron. 135, 153–159.
Zhang, Y., Hu, Y., Wilson, G.S., Moatti-Sirat, D., Poitout, V., Reach, G., 1994. Anal. Chem. 66, 1183–1188.
Zheng, D., Vashist, S.K., Al-Rubeaan, K., Luong, J.H.T., Sheu, F.S., 2012. Analyst 137, 3800–3805.
Zhou, J., Ma, Z., Hong, X., Wu, H.M., Ma, S.Y., Li, Y., Chen, D.J., Yu, H.Y., Huang, X.J., 2019. ACS Sens. 4, 931–937.